INTERNATIONAL JOURNAL FOR NUMERICAL METHODS IN FLUIDS, VOL. 17, 905–920 (1993)

NUMERICAL COMPUTATIONS OF TWO-DIMENSIONAL SOLITARY WAVES GENERATED BY MOVING DISTURBANCES

YUSONG CAO AND ROBERT F. BECK

Department of Naval Architecture and Marine Engineering, The University of Michigan, Ann Arbor, MI 48109, U.S.A.

AND

WILLIAM W. SCHULTZ

Department of Mechanical Engineering and Applied Mechanics, The University of Michigan, Ann Arbor, MI 48109, U.S.A.

SUMMARY

Two-dimensional solitary waves generated by disturbances moving near the critical speed in shallow water are computed by a time-stepping procedure combined with a desingularized boundary integral method for irrotational flow. The fully non-linear kinematic and dynamic free-surface boundary conditions and the exact rigid body surface condition are employed. Three types of moving disturbances are considered: a pressure on the free surface, a change in bottom topography and a submerged cylinder. The results for the free surface pressure are compared to the results computed using a lower-dimensional model, i.e. the forced Korteweg–de Vries (fKdV) equation. The fully non-linear model predicts the upstream runaway solitons for all three types of disturbances moving near the critical speed. The predictions agree with those by the fKdV equation for a weak pressure disturbance. For a strong disturbance, the fully non-linear model predicts larger solitons than the fKdV equation. The fully non-linear calculations show that a free surface pressure generates significantly larger waves than that for a bottom bump with an identical non-dimensional forcing function in the fKdV equation. These waves can be very steep and break either upstream or downstream of the disturbance.

KEY WORDS Solitary waves Korteweg–de Vries equation

1. INTRODUCTION

A disturbance moving steadily at a speed near the transcritical speed in shallow water can periodically generate a succession of solitary waves advancing upstream of the disturbance. A train of weakly non-linear and weakly dispersive waves develops downstream of a region of depressed water surface trailing just behind the disturbance. Although the disturbance is steady (moving at a constant speed), the flow generated never reaches a steady state. Thews and Landweber (cited in Ertekin *et al.*[1]) were the first to mention this phenomenon. This phenomenon was rediscovered numerically by Wu and Wu[2] using a generalized Boussinesq model for long waves generated by a moving-surface pressure distribution or bottom bump. Since then, many theoretical studies and objective experiments have been conducted to understand better the phenomenon.[1,3–7] These studies find that the inclusion of non-linear terms in the free-surface boundary conditions is necessary to predict the solitary waves.

0271–2091/93/220905–16$13.00

Received 10 March 1992
Revised 29 June 1993

Most theoretical studies of this phenomenon are based on perturbation methods. The generalized Boussinesq model[2] is good for long waves (i.e. $\varepsilon = h_0/\lambda$ is small, where h_0 is the mean water depth and λ is a typical wavelength). For a weak disturbance near the critical speed, a simplified forced Korteweg–de Vries (fKdV) equation derived from the Boussinesq equation can be used to model approximately the phenomenon.[4–7] A higher-order model has been developed by Dommermuth and Yue.[8] Ertekin *et al.*[1,3] used the Green–Naghdi fluid sheet equations. Studies have also been extended to three-dimensional shallow water waves.[1,9,10] One common feature of the above formulations is that they require small vertical variations of the flow.

Recently, Protopopov[11] studied solitons generated by a moving-surface pressure using a two-dimensional potential flow model and fully non-linear free-surface boundary conditions. In his study, Protopopov employed a transformation which maps the vertical co-ordinate from $-h(x, t) \leq y \leq \eta(x, t)$ to a rectangular column, $-1 \leq Y \leq 0$, where $h(x, t)$ is the bottom profile. The problem was then solved by a finite differnce method. Choi *et al.*[12] studied the generation of solitons by a three-dimensional ship moving in a channel using a finite element method based on Luke's variational principle. These numerical methods fully consider the vertical variation of the flow. However, because of the co-ordinate transformation, Protopopov's method cannot handle the case in which the disturbance is a submerged body, while the finite element method[12] requires volume integrals and hence is computationally intensive.

In this paper, we present a simple numerical method to compute the waves generated by a disturbance moving near the critical speed using a fully non-linear model (with the complete Laplace field equation and fully non-linear free-surface boundary conditions). The problem is solved in the time domain using a time-stepping procedure combined with a two-dimensional version of the desingularized boundary integral method described in Cao *et al.*[13] The results are compared to those obtained using Wu's fKdV model.[7] We show similar results to the fKdV when the forcing is small, but significant differences appear for larger forcing.

2. PROBLEM FORMULATION

We assume that the flow is two-dimensional, incompressible and irrotational. Then the fluid velocity $\mathbf{u}$ is given by $\mathbf{u}(\mathbf{x}, t) = \nabla\phi$, where $\phi(\mathbf{x}, t)$ is the velocity potential, $\mathbf{x} = (x, y)$ is the spatial location, and t is time. As shown in Figure 1, the co-ordinate system is fixed relative to the

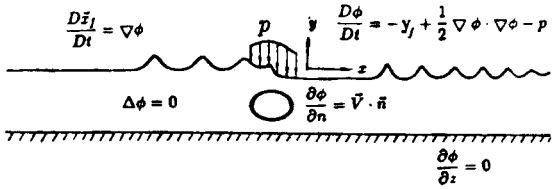

Initial Conditions

$$\phi(x) = 0.0 \qquad (t \leq 0)$$

$$y_f = -p(x, 0) \qquad (t \leq 0)$$

Figure 1. The co-ordinate system and problem definition

undisturbed fluid far up- or down-stream. The y-axis points upwards starting from the undisturbed free surface. The problem is non-dimensionalized based on the undisturbed water depth, the gravitational acceleration and the fluid density. Surface tension is neglected.

The problem is treated as an initial boundary value problem with the motion of the disturbance starting from rest. The fluid domain D is bounded on top by the free surface S_f, internally by the body surface S_h, below by a bottom surface S_b and an enclosing contour S_∞ at infinity.

The continuity equation requires that the potential ϕ satisfies the Laplace equation,

$$\Delta\phi = 0 \quad (\text{in } D). \tag{1}$$

Since the free-surface boundary is not known *a priori*, two boundary conditions are required on it. The kinematic condition requires that a fluid particle remains on the free surface,

$$\frac{D\mathbf{X}_f}{Dt} = \nabla\phi \quad (\text{on } S_f), \tag{2}$$

where

$$\frac{D}{Dt} = \frac{\partial}{\partial t} + \nabla\phi \cdot \nabla$$

is the substantial derivative following a fluid particle and $\mathbf{X}_f = (x_f, y_f)$ is the position vector of a free-surface particle. The dynamic condition requires that the pressure on the free surface equals the ambient pressure $p_a(x, y, t)$ which is assumed to be given. Applying the Bernoulli equation to the free surface gives

$$\frac{D\phi}{Dt} = -y_f + \tfrac{1}{2}|\nabla\phi|^2 - p_a \quad (\text{on } S_f). \tag{3}$$

On the body surface S_h and the bottom S_b, the flow satisfies the non-penetration condition,

$$\frac{\partial\phi}{\partial n_h} = \mathbf{V}_h \cdot \mathbf{n}_h \quad (\text{on } S_h), \tag{4}$$

$$\frac{\partial\phi}{\partial n_b} = \mathbf{V}_b \cdot \mathbf{n}_b \quad (\text{on } S_b), \tag{5}$$

where $\mathbf{V}_h$ and $\mathbf{V}_b$ are the velocities of body surface and the bottom surface, and $\mathbf{n}_h$ and $\mathbf{n}_b$ are the outward (from the fluid domain) unit normal vectors of the two surfaces, respectively. Finally, we use initial conditions for the flow starting from rest,

$$\phi = 0 \quad (\text{in } D \text{ for } t \leq 0) \tag{6}$$

and

$$\eta = -p_0(x) \quad (\text{on } S_f \text{ for } t \leq 0), \tag{7}$$

where $p_0(x)$ is the initial free-surface pressure. The initial rigid body position is also known.

This formulation is exact under the potential flow assumption. No additional assumptions, such as the linearization of the free-surface conditions, are made.

3. FULLY NON-LINEAR COMPUTATION

The problem is solved using a mixed Eulerian–Lagrangian time-stepping procedure.[14] At each time step, the free surface and body positions are known. The velocity potential on the free surface

and the normal velocity on the body surface are also known. Thus, a boundary value problem (BVP) can be solved to determine the free-surface velocity as well as the potential on the body. Then the free-surface potential and position are explicitly updated by time integration of the free-surface kinematic and dynamic boundary conditions (2) and (3), respectively.

The BVP is solved using a desingularized method,[13] where the fundamental singularities are moved away from the boundary surfaces to outside the fluid domain, resulting in a desingularized boundary integral equation. The method has many advantages over the conventional singular boundary integral equation methods. Desingularization allows panel integration of distributed sources to be replaced by a summation of simple sources. It greatly simplifies the logic and allows straightforward vectorization, parallel computation and easy extension to fast O(N) methods. The desingularization distance is determined based on the local grid size so that the algebraic system is still adequately well-conditioned to allow efficient and accurate solutions by iteration. The method can easily handle irregular grids.

In this paper, we use the indirect desingularized method.[13] The velocity potential is contructed by a source distribution over a surface inside the body and a surface above the free surface. The strength of the source distribution is determined by satisfying boundary conditions on the body surface and the free surface. Therefore, we write the velocity potential as

$$\phi(x, y)=\sum_{j=1}^{N^{\mathrm{f}}} \sigma_j^{\mathrm{f}}\Phi^{\mathrm{f}}(x, y; x_j^{\mathrm{f}}, y_j^{\mathrm{f}})+\sum_{k=1}^{N^{\mathrm{h}}} \sigma_k^{\mathrm{h}}\Phi^{\mathrm{h}}(x, y; x_k^{\mathrm{h}}, y_k^{\mathrm{h}}), \tag{8}$$

where (x, y) is the field point, Φ^{f} is the potential due to the source at point $(x_j^{\mathrm{f}}, y_j^{\mathrm{f}})$ above the free surface and its image reflected about the $y=-1$ plane, and Φ^{h} is the potential due to the source at point $(x_k^{\mathrm{h}}, y_k^{\mathrm{h}})$ inside the rigid body surface and its image:

$$\Phi^{\mathrm{f}}=\log[(x-x_j^{\mathrm{f}})^2+(y-y_j^{\mathrm{f}})^2]+\log[(x-x_j^{\mathrm{f}})^2+(y-y_j^{\mathrm{f}}+2)^2], \tag{9}$$

$$\Phi^{\mathrm{h}}=\log[(x-x_k^{\mathrm{h}})^2+(y-y_k^{\mathrm{h}})^2]+\log[(x-x_k^{\mathrm{h}})^2+(y-y_k^{\mathrm{h}}+2)^2]. \tag{10}$$

The function $\phi(x, y)$ automatically satisfies the Laplace equation and the boundary condition on a horizontal bottom except in the area of a bottom bump. The Dirichlet condition on the free surface and the Neumann condition on other rigid body surfaces remains to be satisfied. The source strengths σ_j^{f} and σ_k^{h} are determined by satisfying the boundary conditions at the chosen collocation points on the free surface and the rigid body surface. Thus,

$$\sum_{j=1}^{N^{\mathrm{f}}} \sigma_j^{\mathrm{f}}\Phi^{\mathrm{f}}(\bar{x}_i, \bar{y}_i; x_j^{\mathrm{f}}, y_j^{\mathrm{f}})+\sum_{k=1}^{N^{\mathrm{h}}} \sigma_k^{\mathrm{h}}\Phi^{\mathrm{h}}(\bar{x}_i, \bar{y}_i; x_k^{\mathrm{h}}, y_k^{\mathrm{h}})=\phi_0(\bar{x}_i, \bar{y}_i) \quad (i=1, 2, \ldots, N^{\mathrm{f}}), \tag{11}$$

$$\sum_{j=1}^{N^{\mathrm{f}}} \sigma_j^{\mathrm{f}}\frac{\partial}{\partial n}\Phi^{\mathrm{f}}(\hat{x}_l, \hat{y}_l; x_j^{\mathrm{f}}, y_j^{\mathrm{f}})+\sum_{k=1}^{N^{\mathrm{h}}} \sigma_k^{\mathrm{h}}\frac{\partial}{\partial n}\Phi^{\mathrm{h}}(\hat{x}_l, \hat{y}_l; x_k^{\mathrm{h}}, y_k^{\mathrm{h}})=\mathbf{V}_h\cdot\mathbf{n}(\hat{x}_l, \hat{y}_l) \quad (l=1, 2, \ldots, N^{\mathrm{h}}), \tag{12}$$

where $(\bar{x}_i, \bar{y}_i)$ is a collocation point on the free surface (which is also a fluid particle) and $(\hat{x}_l, \hat{y}_l)$ is a collocation point on the rigid body surface. A source point is placed at a distance from the corresponding collocation point in the normal direction of the surface. The distance between the collocation point and the source point L_{d} is chosen as

$$L_{\mathrm{d}}=l_{\mathrm{d}}s^{\alpha}, \tag{13}$$

where s is the local grid size defined as the average of the distances to both adjacent collocation points, l_{d} is the desingularization factor (constant) which reflects how far the boundary integral

equation is desingularized, and α is a parameter that must be chosen carefully. Equation (13) implies that as the grid becomes finer, the singular points become closer to the boundary (for $\alpha > 0$) In the limit (as the grid size approaches zero), the non-singular integral equation is globally consistent with the singular integral equation although the kernels in the non-singular equation never become singular. The parameter α reflects how fast the singular points approach the boundary as the grid size is refined and will affect the accuracy of the numerical representation of the integral equation. Here, we choose $l_d = 1{\cdot}0$ and $\alpha = 0{\cdot}5$ based on the results of previous numerical studies.[13]

The collocation points on the rigid body surface are uniformly distributed. On the free surface, the collocation points correspond to fluid particles and are uniformly distributed at $t = 0$. As the waves move, the space between the collocation points changes. It is known that fluid particles tend to group near the wave crests where the surface slope has a rapid spatial gradients. Therefore, we have a computational grid which is finer near the crests and coarser near the troughs. With the use of equation (13), the desingularization distance is smaller near the crests, i.e. the source points are closer to the free surface. This allows the method to capture better the rapid change of the flow near the crests.

The function ϕ_0 in equation (11) is known from the previous time step. The combination of equations (11) and (12) yields a system of $N = (N^f + N^h)$ linear algebraic equations. After solving the systems (11), (12) for σ_j^f and σ_k^h, the flow is determined and the flow velocities can be calculated from the analytical spatial derivatives of ϕ in equation (8). The free-surface position and the flow potential can then be updated. The pressure on the body can also be calculated using the Bernoulli's equation and integrating the pressure gives the forces on the body. The linear algebraic system (11), (12) is solved iteratively by a Generalized Minimal Residual Algorithm (GMRES).[13]

The fourth-order Runge–Kutta–Fehlberg method is employed in the time stepping. A fixed co-ordinate system is used with a shifting computational window similar to that in Lee *et al.*[4] for the fKdV equation. The time step Δt and the shifted distance Δx (usually the grid size upstream of the computational domain) are chosen such that

$$J = \frac{\Delta x}{Fr \Delta t} \tag{14}$$

is an integer ($J = 1, 2, 3, \ldots$), where Fr is the Froude number (non-dimensional speed of the disturbance). The window shifts every J time steps. If we view the solution only when the window shifts, the position of the disturbance in relation to the window does not change. When the window shifts, one computational node is dropped at the downstream side of the window without any treatment since no spatial derivative of the free surface is required in this algorithm. This does not cause significant non-physical wave reflection from the downstream open boundary.[13] The position and potential of the incoming computatinal nodes are required and pre-computed using some extra upstream points outside the window. These points are convected by the computed source strengths inside the computational window and do not contribute to the discretized integral equation.

The effects of grid size, the error tolerance for the iterative solution of the algebraic system, and the error tolerance for the Runge–Kutta–Fehlberg subroutine have been thoroughly tested. Adequate resolution (within plotting resolution) is obtained when the GMRES tolerance is less than $10^{-8}(N^f + N^f)$, the Runge–Kutta–Fehlberg tolerance is less than 10^{-3}, and the free-surface grid has at least 15 nodes per wave length.

4. THE fKdV EQUATION

The fKdV equation for a free-surface pressure and a bottom bump can be derived from the generalized Boussinesq equations[7] and has the form

$$\eta_t-\left(1+\frac{3}{2}\eta\right)\eta_x-\frac{1}{6}\eta_{xxx}=\frac{1}{2}(p_a+b)_x=\frac{1}{2}P_x, \tag{15}$$

where $p_a=p_a(x+Frt)$ and $b=b(x+Frt)$ represent a free-surface pressure and a bottom profile moving in the x-direction, respectively. Given the forcing and initial conditions, equation (15) can be solved for the wave elevation η.

In the fKdV model, the free-surface pressure and the bottom bump disturbance play the same forcing role, i.e. the waves generated by a pressure disturbance will be the same as the waves due to a bottom-bump disturbance if the two disturbances have the same non-dimensional disturbance distribution. This implies that in an experiment, a free-surface pressure distribution can be replaced by the equivalent bottom bump which is easier to control.[4] However, they are not interchangeable if the parameter ranges are beyond the fKdV assumptions. In addition, the fKdV equation, as well as the Boussinesq equations, cannot accommodate problems with a body moving between the bottom and the free surface.

No closed-form solution to equation (15) has been found and a numerical approach is necessary. Numerical instability may occur if the fKdV equation is solved in the form of equation (15). It has been found to be preferable to replace the dispersion term η_{xxx} by η_{xxt} based on the lowest-order solution. Then equation (15) becomes

$$\eta_t-\left(1+\frac{3}{2}\eta\right)\eta_x-\frac{1}{6}\eta_{xxt}=\frac{1}{2}P_x. \tag{16}$$

This was first pointed out by Benjamin *et al.*[15] and used by Wu[7] and Lee *et al.*[4]

Following Wu,[7] for comparison purposes, we also solve the fKdV equation (16) numerically with a time-stepping procedure based on the Euler's predictor–corrector algorithm to advance time without iteration at the correction stage. A second-order central-difference approximation is used for the spatial derivatives. Both the prediction and correction stages reduce to the inversion of a constant tridiagonal matrix, which is strictly diagonally dominant.

The moving computational window technique is employed. Again, when the window shifts, one-node point is dropped at the downstream side of the window and a new point emerges into the window from upstream. Because of the finite computational domain, a treatment for the open boundary conditions is necessary to reduce non-physical reflections from the boundaries. Wu and Wu[2], Wu[7] and Lee *et al.*[4] use

$$\eta_t=\pm\eta_x, \tag{17}$$

where the '+' and '−' are taken for the up- and down-stream conditions, respectively. Although this open boundary condition is only appropriate for linear waves with unit phase speed, it has been shown to reduce most of the non-physical small amplitude wave reflection from open boundaries. The open boundary condition (17) is discretized by forward differencing in time. For the spatial discretization, backward differencing is used for the upstream point and forward differencing for the downstream point. Even though the open boundary condition (17) is used, the value of η for the incoming nodes still needs to be provided. It is not clearly stated how the value of η for the incoming point is provided in the above mentioned papers. We provide the value by quadratic extrapolation using the nearest three points.

5. NUMERICAL RESULTS

5.1. *Solitons due to a free-surface pressure*

To compare the fKdV and fully non-linear models, a cosine pressure distribution used by Wu[7] is chosen,

$$P(x+Frt)=p_a(x+Frt)=\begin{cases}\frac{1}{2}P_m\{1+\cos[\frac{2\pi}{L}(x+Frt)]\} & |x+Frt|\leq\frac{L}{2},\\ 0 & |x+Frt|\geq\frac{L}{2}.\end{cases}$$

First the results by the fKdV and the fully non-linear computations for a relatively weak forcing ($P_m=0{\cdot}02$) moving at the critical speed ($Fr=1$) are compared. Figure 2 shows the waves at different times. The results shown in Figure 2 use 301 node points and a time step $\Delta t=0{\cdot}2$ for both computations. No upstream runaway soliton is observed since the disturbance is weak and the period for the soliton generation is very large. Good agreement between the two models for the upstream wave near the disturbance can be seen although the fully non-linear program predicts a steeper front wave. Downstream, the differences between the waves predicted by the two models are quite significant especially the phase. The waves computed by the fKdV program travel faster downstream away from the disturbance than those by the fully non-linear program.

Although it is difficult to isolate the causes of the differences in the results between the fKdV and the fully non-linear computations, it seems that the differences are mainly due to modelling of

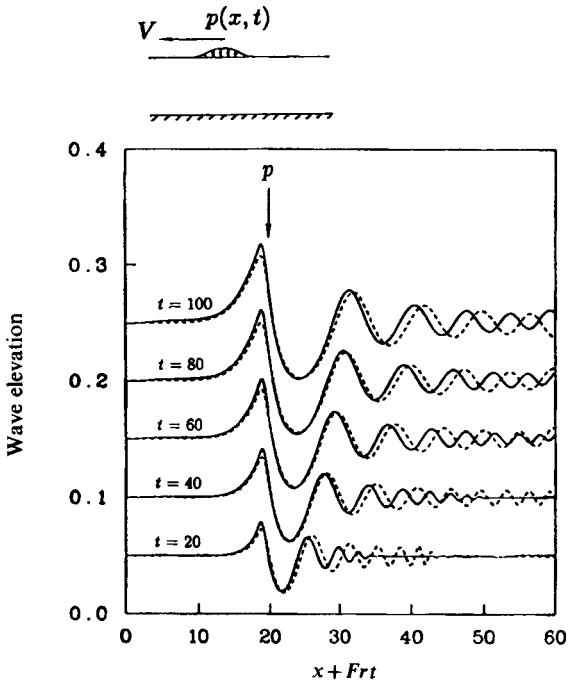

Figure 2. Waves generated by a moving-surface pressure disturbance. In this and the following figures the wave elevation is increased with time artificially for clarity in graphical presentation. The horizontal co-ordinate $x+Frt$ is chosen so the disturbance is fixed. The arrow pointing downwards indicates the centroid of the disturbance. ($P_m=0{\cdot}02$, $Fr=1{\cdot}0$, $\Delta t=0{\cdot}2$, $N^f=301$), (—— fully non-linear model; ------ fKdV model)

the free-surface non-linearity and the vertical flow variation. During the initial transition, the generated waves are small and the bottom effect is negligible and the waves move as if in deep water. The fKdV model overpredicts the bottom effect at this early stage by averaging the flow quantities vertically over the water layer. Therefore, the dispersion relations of the two models result in different wave speeds. In the last time step in Figure 2, both methods start to exhibit a small amount of non-physical reflections at the downstream open boundary. The use of a finer grid changes the results only marginally for both the fKdV and fully non-linear computations.

For a stronger forcing, $P_m = 0{\cdot}1$, both models predict upstream runaway solitons as shown in Figure 3. The two methods are in qualitative agreement. However, the fully non-linear model again predicts steeper waves and a shorter period in generating solitons. The differences become more obvious when the forcing gets stronger. Figure 4 shows the results for $P_m = 0{\cdot}15$. As can be seen, the non-linear model predicts a much steeper front wave which starts to break at $t = 24{\cdot}2$ and causes the computation to stop. For $P_m = 0{\cdot}2$, which is used in Wu[7] and Lee *et al.*,[4] the waves computed by the non-linear program break even sooner (not shown here), while the waves computed by the fKdV model do not break, showing that the fKdV model fails at this higher level of forcing. The derivation of the fKdV equation assumes the non-dimensional forcing P_m must be $O(\varepsilon^4)$.[7] A typical wavelength can be estimated for the case $P_m = 0{\cdot}1$ from Figure 3 to be around 10 and ε is thus approximately 0·1. Therefore, the forcing P_m should be $O(10^{-4})$; the values for P_m used in Wu[7] seem far beyond this limitation. It should also be noted that Lee *et al.*[4] experimentally observed wave breaking for $P_m \geqslant 0{\cdot}15$. Protopopov[11] has also concluded from his numerical study that the pressure must be small ($P_m \leqslant 0{\cdot}1$) in order to obtain accurate results with the use of the generalized Boussinesq equations from which the fKdV is derived.[7]

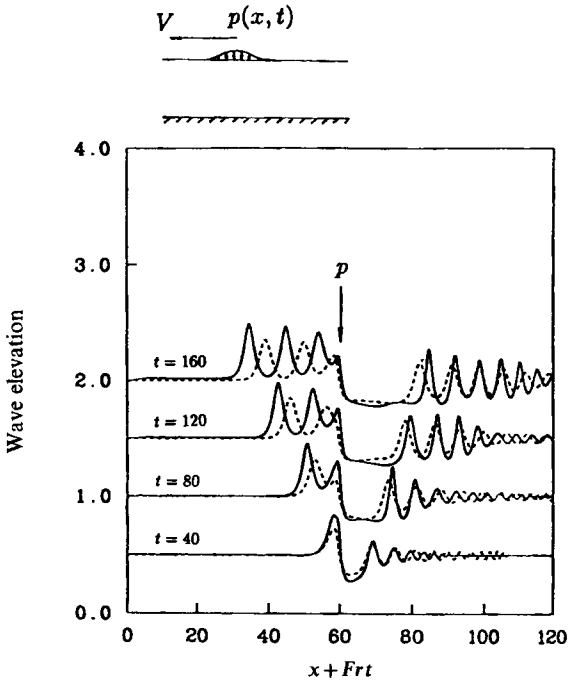

Figure 3. Waves generated by a moving surface pressure disturbance ($P_m = 0{\cdot}1$, $Fr = 1{\cdot}0$, $\Delta t = 0{\cdot}2$, $N^f = 481$), (—— fully non-linear model; – – – – fKdV model)

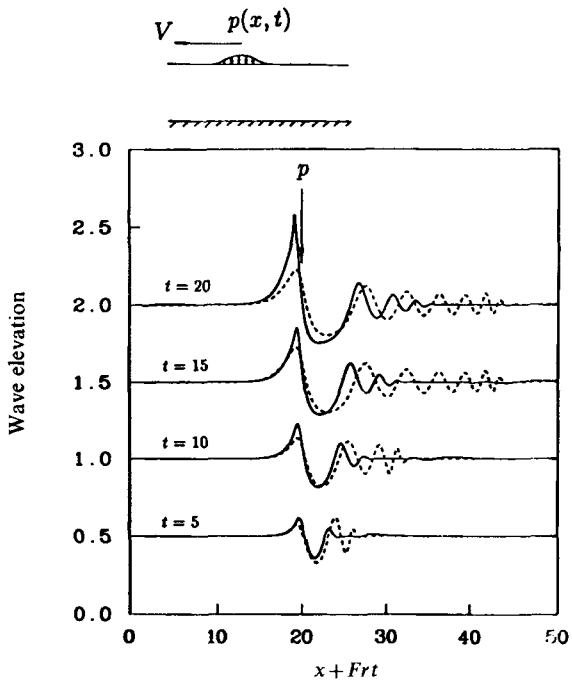

Figure 4. Waves generated by a moving surface pressure disturbance ($P_m=0{\cdot}15$, $Fr=1{\cdot}0$, $\Delta t=0{\cdot}2$, $N^f=101$), (—— fully non-linear model; – – – – – fKdV model)

Figure 5 shows the results for a surface pressure at the supercritical speed ($Fr=1{\cdot}5$). Both models reveal similar wave characteristics. The downstream transient waves travel at slower speeds than the disturbance and eventually only a single steady soliton remains travelling at the same speed as the forcing. Furthermore, since the flow is not in resonance, the soliton height is smaller than those generated by the disturbances moving near the critical speed.

5.2. Comparison of free-surface pressure and bottom topography

In the fKdV model, the waves due to a pressure disturbance are the same as the waves due to bottom topography if their dimensionless disturbance distributions are identical. This is due to the fact that the fKdV model assumes small ε and uses the vertical average of the flow velocity over the water layer. The differences in the waves generated by the free surface pressure and the bottom bump of identical disturbance distribution are now examined using the fully non-linear model.

Figure 6 shows the waves due to a semi-elliptical bottom bump moving at $Fr=1$. The major axis L and minor axis b_0 are 2·0 and 0·2, respectively. Figure 7 shows the waves generated by the same non-dimensional semi-elliptical distribution of free-surface pressure as the bottom bump. The waves shown in Figure 6 and 7 are computed using the fully non-linear model. For the fKdV equation, the bottom bump and the free-surface pressure would have exactly the same right-hand-side forcing function. Thus, the predicted waves using the fKdV equation would be identical for the two cases. Comparing Figures 6 and 7 shows the waves generated by the two types of disturbances are significantly different. The free-surface pressure behaves as a stronger forcing

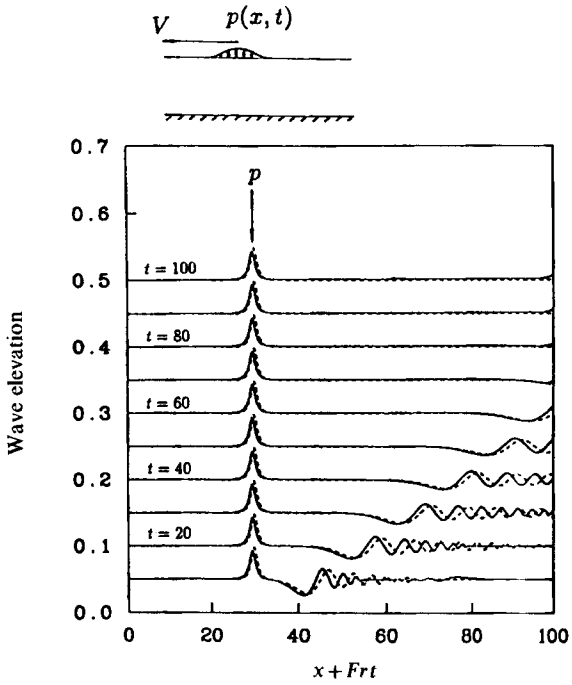

Figure 5. Waves generated by a moving surface pressure disturbance ($P_m = 0{\cdot}1$, $Fr = 1{\cdot}5$, $\Delta t = 0{\cdot}2$, $N^f = 251$), (—— fully non-linear model; ------ fKdV model)

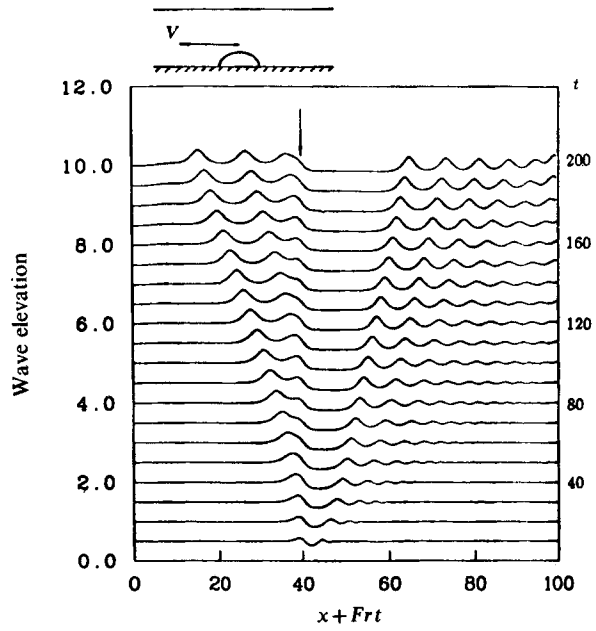

Figure 6. Waves generated by a moving bottom bump of elliptical cross-section ($P_m = 0{\cdot}5$, $b_0 = R_y = 0{\cdot}1$, $L = 2R_x = 2{\cdot}0$, $Fr = 1{\cdot}0$, $\Delta t = 0{\cdot}2$, $N^f = 251$, $N^b = 20$, fully non-linear model)

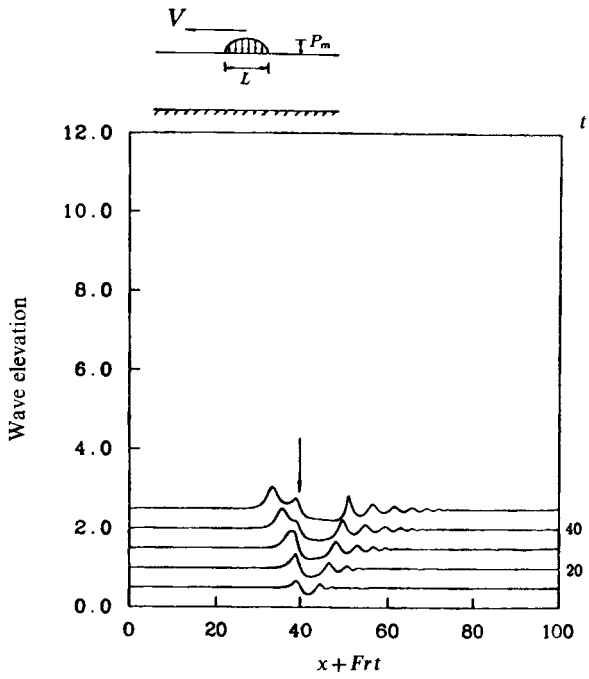

Figure 7. Waves generated by a moving surface pressure with an elliptical distribution ($P_m=0{\cdot}1$, $L=2{\cdot}0$, $Fr=1{\cdot}0$, $\Delta t=0{\cdot}2$, $N^f=251$, fully non-linear model)

than the bottom bump. The waves due to the pressure forcing start to break at about $t=55$. The breaking occurs at the first wave crest downstream of the disturbance. Figure 8 shows the velocity vector field for the same case as in Figure 7 for three regions: (a) the region ahead of the disturbance ($30{\cdot}0<x+Frt<41{\cdot}2$), (b) the region of the depressed water surface just behind the disturbance ($41{\cdot}2<x+Frt<48{\cdot}9$) and (c) the region of the downstream wave trains ($48{\cdot}9<x+Frt<59{\cdot}0$). As can be seen, the vertical variation is very significant (especially near the wave crests), except that the flow behaves like a uniform current in the region of the depressed water surface behind the disturbance and ahead of the first downstream wave crest. The free-surface particles (dots on the free surface in Figure 8) tend to group around the crest as expected.

5.3. Solitons due to submerged cylinders

The fKdV equation cannot be used to compute waves generated by a submerged cylinder, but the fully non-linear model easily can. Figure 9 shows the waves due to a circular cylinder with the radius $R=0{\cdot}15$ moving at $Fr=1{\cdot}0$ and centroid depth of $d=0{\cdot}6$. The generation of solitons is clearly seen. Figure 10 shows the waves generated by a larger circular cylinder with $R=0{\cdot}2$ at the same speed. The cylinder with larger radius implies a stronger disturbance and therefore produces larger waves and the first wave downstream starts to break at about $t=45$. Figure 11 shows the waves due to a cylinder ($R=0{\cdot}15$) moving at the supercritical speed ($Fr=1{\cdot}5$). Again only a single soliton eventually moves with the disturbance as in the case of surface pressure (Figure 5). Figures 12 and 13 show the waves due to elliptical cylinders. In the first case, the ratio of the major axis to

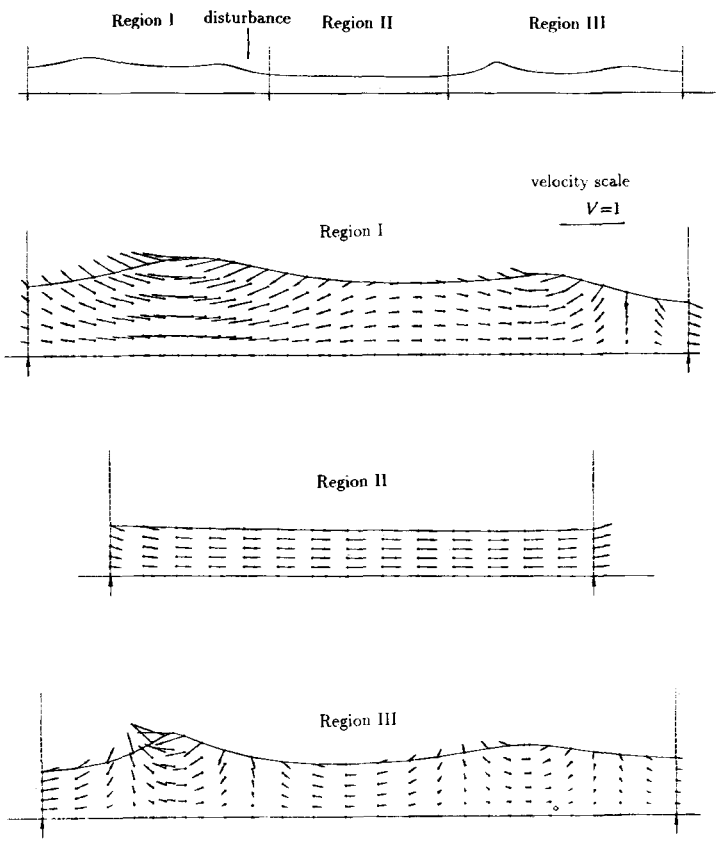

Figure 8. Velocity vector of the flow fluid (same as in Figure 7) in the three regions: Region I: ahead of the disturbance ($30{\cdot}0 < x + Frt < 41{\cdot}2$). Region II: the depressed water surface behind the disturbance ($41{\cdot}2 < x + Frt < 48{\cdot}9$). Region III: the downstream wave trains ($48{\cdot}9 < x + Frt < 59{\cdot}0$). (The dots indicate the points at which the velocity is calculated, while the arrows indicate the magnitude and direction of the velocity vectors)

the minor axis is $R_y/R_x = 0{\cdot}075$. In the second case, the cylinder has a larger minor axis ($R_y/R_x = 0{\cdot}1$). This stronger disturbance causes breaking of the first downstream wave.

Our fully non-linear computations (as well as the fKdV computations) stop when wave profiles become sharply peaked to suggest wave breaking. Since wave breaking is a very complicated process, we do not attempt to model the breaking process or the flow after the breaking and no special treatment for breaking waves has been developed. The program stops when the wave slope near a crest reaches a value for which the time-stepping procedure can no longer converge to a given tolerance. Increasing the spatial and temporal resolution does not significantly change the time when the crest forms and the algorithm does not converge. The desingularized method has been applied to the sharp edges of Karman–Trefftz airfoil (without a free surface) and found to give very good agreement with the analytic solution as long as there is no collocation point at the corners.[16] The formation of sharp crests cause inaccuracy in the desingularized soution, but our experiences show other boundary integral techniques perform just as poorly at the corners. The development of techniques to allow computation to continue in the presence of wave breaking is the topic of further research.

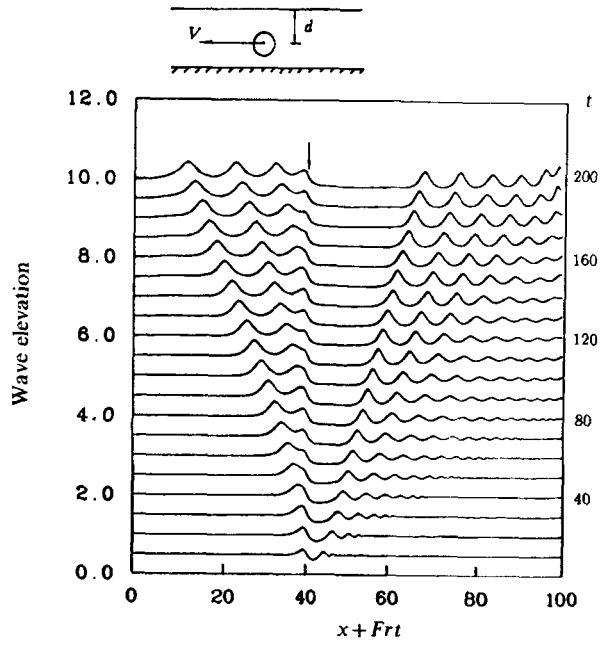

Figure 9. Waves generated by a submerged circular cylinder ($R=0{\cdot}15$, $d=0{\cdot}6$, $Fr=1{\cdot}0$, $\Delta t=0{\cdot}2$, $N^{f}=251$, $N^{b}=30$, fully non-linear model)

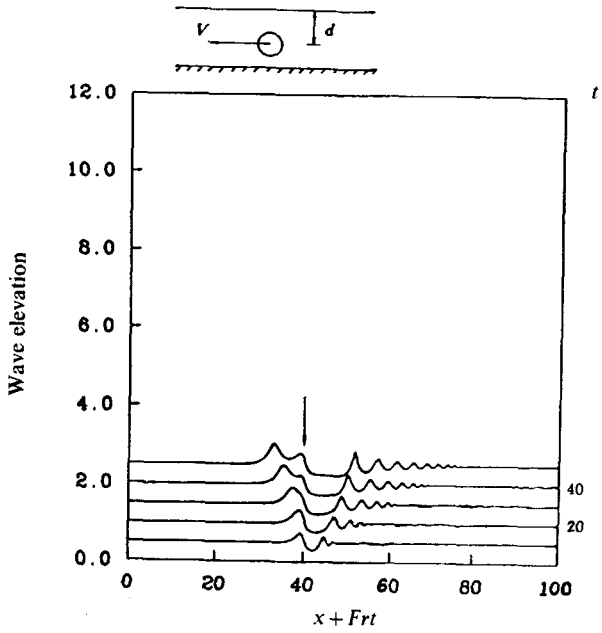

Figure 10. Waves generated by a submerged circular cylinder ($R=0{\cdot}2$, $d=0{\cdot}6$, $Fr=1{\cdot}0$, $\Delta t=0{\cdot}2$, $N^{f}=251$, $N^{b}=30$, fully non-linear model)

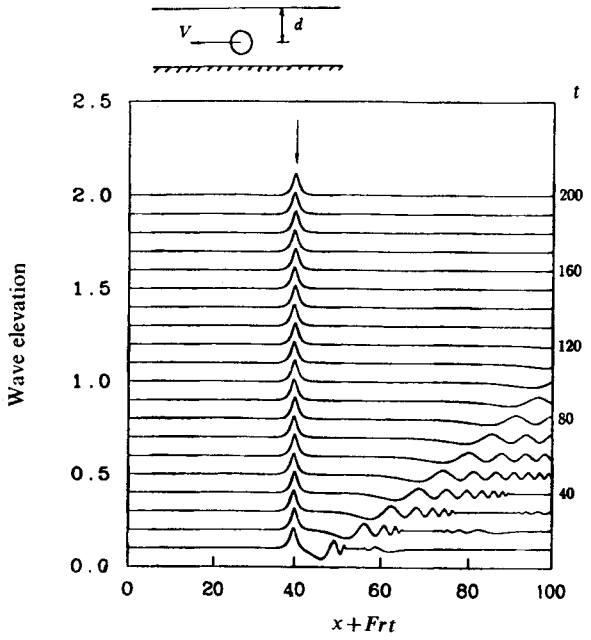

Figure 11. Waves generated by a submerged circular cylinder ($R=0{\cdot}15$, $d=0{\cdot}6$, $Fr=1{\cdot}5$, $\Delta t=0{\cdot}2$, $N^{f}=251$, $N^{b}=30$, fully non-linear model)

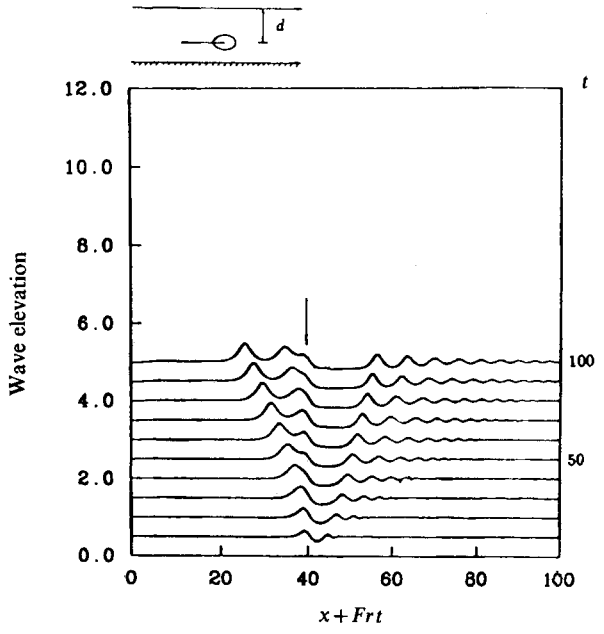

Figure 12. Waves generated by a submerged elliptical cylinder ($R_x=1{\cdot}0$, $R_y=0{\cdot}075$, $d=0{\cdot}6$, $Fr=1{\cdot}0$, $\Delta t=0{\cdot}2$, $N^{f}=251$, $N^{b}=35$, fully non-linear model)

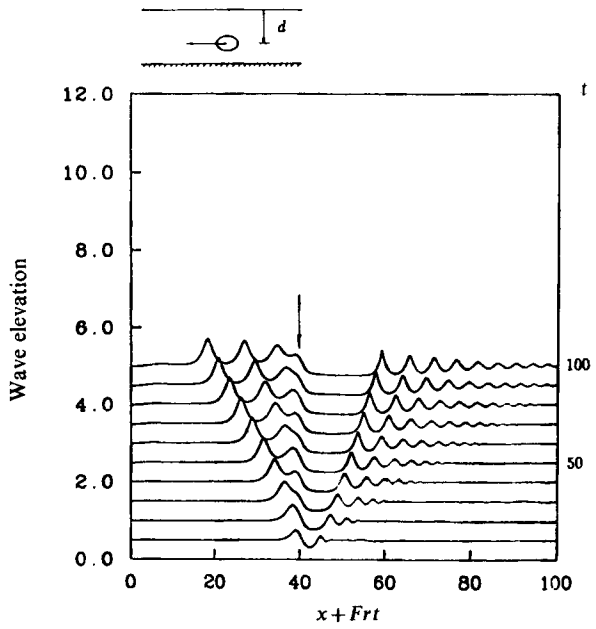

Figure 13. Waves generated by a submerged elliptical cylinder ($R_x=1{\cdot}0$, $R_y=0{\cdot}1$, $d=0{\cdot}6$, $Fr=1{\cdot}0$, $\Delta t=0{\cdot}2$, $N^t=251$, $N^b=35$, fully non-linear model)

6. CONCLUSIONS

The fully non-linear model predicts upstream runaway solitons for three types of disturbances moving near the critical speed. The numerical results from the fully non-linear model agree with the fKdV results for a weak surface pressure disturbance. For stronger disturbances, the fully non-linear model predicts larger solitons than the fKdV model. These solitons are so steep that they break either upstream or downstream. The fully non-linear calculations show significant differences in the wave patterns caused by free-surface pressure disturbances and by bottom topographical disturbances. In contrast, the fKdV equation predicts no difference in the waves generated by the two different types of disturbances.

ACKNOWLEDGEMENTS

This work was supported under the Program in Ship Hydrodynamics at The University of Michigan, funded by The University Research Initiative of the Office of Naval Research, Contract Number N000184-86-K-0684. Computations were made in part using a CRAY Grant, University Research and Development Program at the San Diego Supercomputer Center.

REFERENCES

1. R. C. Ertekin, W. C. Webster and J. V. Wehausen, 'Waves caused by a moving disturbance in a shallow channel of finite depth', *J. Fluid Mech.*, **169**, 275–292 (1986).
2. D. M. Wu and T. Y. Wu, 'Three-dimensional nonlinear long waves due to surface pressure', *Proc. 14th Symp. on Naval Hydrodynamics*, National Academy Press, Washington DC, 1982.

3. R. C. Ertekin, W. C. Webster and J. V. Wehausen, 'Ship-generated solitons', *Proc. 15th Symp. on Naval Hydrodynamics*, National Academy Press, Washington DC, 1985, pp. 347–364.
4. S. J. Lee, G. T. Yates and T. Y. Wu, 'Experiments and analyses of upstream-advancing solitary waves generated by moving disturbances', *J. Fluid Mech.*, **199,** 569–593 (1989).
5. T. R. Akylas, 'On the excitation of long nonlinear water waves by a moving pressure disturbance', *J. Fluid Mech.*, **141,** 455–466 (1984).
6. S. L. Cole, 'Transient waves produced by flow past a bump', *Wave Motion*, **7,** 579–587 (1985).
7. T. Y. Wu, 'Generation of upstream-advancing solitons by moving disturbances', *J. Fluid Mech.*, **184,** 75–99 (1987).
8. D. G. Dommermuth and D. K. P. Yue, 'A high-order spectral method for the study of non-linear gravity waves', *J. Fluid Mech.*, **184,** 267–288 (1987).
9. C. C. Mei, 'Radiation of solitons by slender bodies advancing in a shallow channel', *J. Fluid Mech.*, **162,** 53–67 (1986).
10. C. Katsis and T. R. Akylas, 'On the excitation of long nonlinear water waves by a pressure distribution. Part 2. Three-dimensional effects', *J. Fluid Mech.*, **177,** 49–65 (1987).
11. B. E. Protopopov, 'Numerical investigation of soliton generation by a moving region of free surface pressure', *Int. Ser. Numer. Math.*, **99** (1991).
12. H. S. Choi, K. J. Bai, J. W. Kim and H. Cho, 'Nonlinear free surface waves due to a ship moving near the critical speed in a shallow water', *Proc. 18th Symp. on Naval Hydrodynamics*, National Academy Press, Washington DC, 1991, pp. 173–190.
13. Y. Cao, W. W. Schultz and R. F. Beck, 'Three-dimensional desingularized boundary integral methods for potential problems', *Int. j. numer. methods fluids*, **12,** 785–803 (1991).
14. Y. Cao, W. W. Schultz and R. F. Beck, 'Three-dimensional, unsteady computations of non-linear waves caused by underwater disturbance', *Proc. 18th Symp. on Naval Hydrodynamics*, National Academy Press, Washington DC, 1991, pp. 417–425.
15. T. B. Benjamin, J. L. Bona and J. J. Mahony, 'Model equations for long waves in nonlinear dispersive systems', *Phil. Trans. R. Soc.* **A272,** 47–78 (1972).
16. Y. Cao, T. Lee and R. F. Beck, 'Computation of nonlinear waves generated by floating bodies', *Proc. 7th Int. Workshop on Water Waves and Floating Bodies*, Val de Reuil, France, 1992, pp. 24–27.